Int. J. Solids Structures Vol. 29, No. 9, pp. 1173–1191, 1992
Printed in Great Britain.

0020-7683/92 $5.00 + .00


# NEW EXPLICIT MICROPLANE MODEL FOR CONCRETE: THEORETICAL ASPECTS AND NUMERICAL IMPLEMENTATION

IGNACIO CAROL† and PERE C. PRAT†
School of Civil Engineering, ETSECCPB—Technical University of Catalonia, 08034 Barcelona, Spain

and

ZDENĚK P. BAŽANT
Department of Civil Engineering, Center for Advanced Cement-Based Materials, Northwestern University, Evanston, IL 60208, U.S.A.

(*Received* 2 *April* 1990; *in revised form* 10 *August* 1991)

**Abstract**—The microplane model is a powerful approach for the representation of the complex triaxial behavior of concrete and other similar materials. However, most efforts in previous formulations were devoted to the development of the model itself and to the experimental data fitting, rather than to a comprehensive theoretical description or to attainment of a modular and computationally efficient implementation in a computer code. In this paper, these objectives are pursued. The formulation of the model has been modified to rationalize the structure of the basic hypotheses, simplify the equations and generalize the concepts whenever possible. The result is a new formulation which, while retaining the favorable properties achieved previously, is also easier to understand, and convenient for computer implementation and large-scale calculations. A computational scheme is presented with the unified structure of a general code serving the double purpose of test specimen analysis and finite element analysis. In practice, this structure includes two different main programs which call the same set of constitutive subroutines. A salient feature of the new version of the model is that the computation of the stress corresponding to a prescribed strain increment of finite size is fully explicit. Step-by-step numerical integration, usually necessary for the practical use of constitutive models, can be avoided. Consequently, the complexity of the code and the cost of computations can be dramatically reduced. Some examples of applications, used to verify the previous version of the model, are also presented. They demonstrate that this new formulation gives a much better numerical efficiency for code implementation while keeping the same desirable features and accuracy in experimental data fitting.

## 1. INTRODUCTION

In 1938, G. I. Taylor suggested a new class of material models for plastic polycrystalline metals in which the constitutive material properties are characterized by relations between the stress and strain components on planes of various orientations in the material (now called the microplanes), which are constrained either statically or kinematically to the macro-stress or macro-strain. Based on the static constraint, this basic idea has been extensively developed for metals under the name of slip theory, beginning with the pioneering work of Batdorf and Budianski (1949). Later, the models with static constraint have been adapted for geomaterials (Zienkiewicz and Pande, 1977; Pande and Sharma, 1983). In application to concrete and geomaterials, the name "slip theory" became misleading because most of the inelastic response is due to damage such as microcracking, and the more general term "microplane model" was coined (Bažant and Oh, 1983; Bažant, 1984). It was also recognized that the strain-softening observed in geomaterials cannot be represented with a static constraint because the microplane system becomes unstable, and consequently a kinematic constraint has been adopted (Bažant and Oh, 1983, 1985; Bažant, 1984; Bažant and Gambarova, 1984; Bažant and Prat, 1988), although a more general mixed constraint might conceivably also be used.

The microplane model with kinematic constraint and strain-softening has proved to be a powerful approach for modelling rather complex aspects of triaxial behavior of

† Formerly Visiting Scholars, Center for Advanced Cement-Based Materials, Northwestern University, Evanston, IL 60208, U.S.A.

brittle–plastic materials such as concrete, rock, ceramics and some composites (Bažant and Gambarova, 1984; Bažant and Oh, 1985; Bažant and Prat, 1988; Bažant and Ožbolt, 1990). However, as usual in the exploration of new constitutive models, most attention has so far been paid to achieving an accurate representation of the main aspects of material behavior given by experimental curves rather than to other theoretical or numerical aspects also important for constitutive modelling.

Further work has lead to the conclusion that the theoretical description of the model given in previous works can be simplified, the same concepts can be presented in a more comprehensive way, and a new and clearer interpretation of some of the equations and variables involved in the formulation is possible. Also, some derivations can be given a more rigorous or alternative description, and some changes can be made in the hypotheses and assumptions, so that the final formulation is better suited for practical application.

From the viewpoint of numerical implementation and code development, the previous formulations of the microplane model also lacked a systematic approach. In general, the computer implementation of a constitutive model is undertaken with one of the following two purposes: (i) representation of the material behavior itself, as a relationship between stress and strain ("single-point constitutive verification"), or (ii) representation of the material behavior in the context of structural analysis ("F.E. analysis"). Without a unified scheme of implementation, the programs developed for these two purposes may well have completely different structures, and the part of the code corresponding to the constitutive model may feature two completely different implementations of the same model, which in a way was the case for the previous versions of the microplane model.

In this paper both aspects, a new theoretical description (Section 2) and a new numerical implementation scheme (Section 3) for the microplane model, are presented. Altogether, these aspects yield a new version of the model which, while keeping all the useful features achieved in the previous version in terms of constitutive verification, is also easier to understand and better suited for practical use in the context of a general F.E. code. The new computer scheme includes two model-independent main programs calling the same material subroutine which gives access to all the model-specific routines and computations. In this way, all the inconveniences caused by having two different programs implementing the same model are overcome automatically: the code needs to be written only once, and once verified at the constitutive level it is automatically working for F.E. computations. Moreover, any further modifications introduced to the model need to be encoded only once. Thus, both the single-point and F.E. analysis programs always contain the same version of the model, and the results obtained from both levels of analysis are fully consistent for comparison or complementary use in the same practical problem. By virtue of the general scheme used and the new theoretical assumptions for the model, the computations in these subroutines (which basically must perform a load-step computation from prescribed strain) are fully explicit, without any step-by-step integration procedure. This makes the code simple to implement and fast to run.

Section 4 presents some examples. The results obtained are compared with experimental data and published results of the previous version of the microplane model. The comparison is made in terms of capability to fit experimental data as well as numerical efficiency. Finally, Section 5 gives a brief summary and the main conclusions drawn from this work.

## 2. THEORETICAL DESCRIPTION OF THE EXPLICIT MICROPLANE MODEL

At a point within the material, a *microplane* is defined as an arbitrary plane which cuts through the material at that point, defined by the orientation of its normal unit vector of components $n_i$. The most direct and easiest physical interpretation of a microplane comes from the observation of the material microstructure, as the interface or discontinuity plane between grains or different components in the heterogeneous medium (Bažant and Gambarova, 1984; Bažant and Oh, 1985; Bažant and Prat, 1988).

On a generic microplane, certain components of strains and stresses are considered. These are the normal and shear strains and stresses on that plane. A set of stress–strain laws are defined as the relations between strains and stresses on the microplane. These laws,

together with the relations between macroscopic and microplane stresses and macroscopic and microplane strains, constitute the material model.

2.1. *Kinematically constrained microplane system*

In the first models of this type developed for metals and soils, a static constraint (the microplane stresses are equal to the resolved components of the stress tensor on that plane) was assumed as the fundamental micro–macro relationship. However, to represent the behavior of quasibrittle materials such as concrete or rock, showing strain softening, a kinematic constraint (the microplane strains are equal to the resolved components of the strain tensor on the plane) seems to be necessary. As will be shown in Section 3, this assumption fits very well into the strain-to-stress scheme used for numerical calculations and makes possible fully explicit types of calculations with great economy in computer time.

The theoretical framework for the new explicit microplane model is based on the three hypotheses given below, similar to those used by Bažant and Prat (1988), with some changes that affect the resulting formulation and its numerical implementation:

*Hypothesis I.* The normal and shear (tangential) strains $\varepsilon_N$ and $\varepsilon_{T_r}$ on a microplane of unit normal $n_i$ are the resolved components of the macroscopic strain tensor $\varepsilon_{ij}$ in that direction, which implies that

$$\varepsilon_N = \varepsilon_{ij} n_i n_j \tag{1}$$

$$\varepsilon_{T_r} = \varepsilon_{ij} n_j - \varepsilon_N n_i = (\delta_{ij} - n_i n_j) n_k \varepsilon_{jk}. \tag{2}$$

Additionally, the normal strain is split in two parts, the volumetric strain $\varepsilon_V$ and the (normal) deviatoric strain $\varepsilon_D$, the expressions of which are

$$\varepsilon_V = \varepsilon_{kk}/3 \tag{3}$$

$$\varepsilon_D = \varepsilon_N - \varepsilon_V. \tag{4}$$

The latin lowercase subscripts refer to Cartesian coordinates $x_i (i = 1, 2, 3)$, and subscript repetition implies summation.

Note that the tangential strain is a vector with three components in space, but its direction always lies in the microplane of normal $n_i$ [(check that $\varepsilon_{T_r} n_i = 0$, from eqn (2)]. Also the normal strains are vectors with three Cartesian components in the normal direction $n_i$, though only their magnitudes $\varepsilon_N$, $\varepsilon_V$ and $\varepsilon_D$ are used. A useful alternative interpretation of the variables $\varepsilon_V$, $\varepsilon_D$ and $\varepsilon_{T_r}$ can be obtained if they are derived in terms of the volumetric $\varepsilon_V$ and deviatoric $e_{ij} = \varepsilon_{ij} - \varepsilon_V \delta_{ij}$ parts of the macroscopic strain instead of directly from the tensor $\varepsilon_{ij}$. Then, the volumetric strain at microplane level $\varepsilon_V$, which is the same for all the microplanes, is directly equal to the macroscopic volumetric strain. The normal deviatoric strain $\varepsilon_D$ and the tangential strain $\varepsilon_{T_r}$, which are different for each microplane, are equal to the normal and tangential components of the projection of the deviatoric strain tensor, $e_{ij}$, on the microplane considered.

*Hypothesis II.* Associated with the three strains $\varepsilon_V$, $\varepsilon_D$ and $\varepsilon_{T_r}$, the three corresponding stresses $\sigma_V$, $\sigma_D$ and $\sigma_{T_r}$ are introduced so that their respective products give directly the work done on the microplane. The strain–stress laws at this level are a set of empirical relationships defining the evolution of each one of those three stresses as a function of the three microplane strains (and possibly their history) exclusively.

The fact that the laws for $\sigma_V$, $\sigma_D$ and $\sigma_{T_r}$ are functions of strains exclusively is a very important difference with the previous version of the model (Bažant and Prat, 1988). This hypothesis permits the model to be fully kinematically constrained. Consequently, other kinds of dependences, such as the dependence of $\sigma_{T_r}$ on a certain invariant of the macroscopic

stress tensor assumed in previous works (which in fact established a "mixed" kinematic–static constraint for the model) are in this case excluded from the formulation.

*Hypothesis III.* The relationship between the microplane stresses $\sigma_V$, $\sigma_D$ and $\sigma_{T_r}$ and the macroscopic stress tensor $\sigma_{ij}$ is obtained by applying the principle of virtual work. Its application to this case is explained in some detail in Appendix A, including certain considerations about symmetry requirements for the tensors $\sigma_{ij}$ and $\varepsilon_{ij}$ necessary to ensure interchangeability of the indices $i$ and $j$ in the final expressions (the symmetry considerations used in the Appendix are an alternative to the *a priori* symmetrization of eqn (2) used in previous works to reach the same final effect). The expression for the macroscopic stress is then:

$$\sigma_{ij} = \sigma_V \delta_{ij} + \frac{3}{2\pi}\int_\Omega \sigma_D n_i n_j \, d\Omega + \frac{3}{2\pi}\int_\Omega \frac{\sigma_{T_r}}{2}(n_i\delta_{rj} + n_j\delta_{ri} - 2n_i n_j n_r)\, d\Omega \tag{5}$$

where the integral domain represented by $\Omega$ represents the upper half hemisphere and $\delta_{ij}$ is the Kronecker delta.

An important new feature of eqn (5) is that it is written in terms of the total values of stresses instead of differential increments. The equation would also be valid if all the stress variables were replaced by their differential increments, which was how it was presented in the original formulation (Bažant and Prat, 1988). If, however, the equation is written in terms of the total values, then the current (total) value of the macroscopic stress tensor $\sigma_{ij}$ can be obtained from the current (total) values of the microplane stresses $\sigma_V$, $\sigma_D$ and $\sigma_{T_r}$ at any moment during the load history, by direct application of eqn 5. This desirable feature cannot be obtained from the incremental-type equation.

Another advantageous aspect of eqn (5) is that is permits a clear interpretation of the contribution of each of the microplane stresses ($\sigma_V$, $\sigma_D$ and $\sigma_{T_r}$) to the macroscopic stress tensor $\sigma_{ij}$. From that equation, one can see that the $\sigma_V$ term gives a volumetric contribution to $\sigma_{ij}$, and the $\sigma_{T_r}$ term gives a pure deviatoric contribution to the macroscopic stress tensor (this becomes clear by noting that this term becomes zero if $i = j$). The $\sigma_D$ term is the only one which gives both volumetric and deviatoric contributions to the macroscopic stress tensor. Consequently, this term is responsible for the intrinsic coupling the model shows between volumetric and deviatoric behavior, such as deviatoric-induced dilatancy, etc.

With the three hypotheses presented, and provided that specific definition of the microplane stress–strain relationships is given according to Hypothesis II, the basic framework of the model is complete and it is already possible to calculate the macroscopic stresses which correspond to a prescribed value of macroscopic strains [see the scheme in Fig. (1)]: from the macroscopic strain increment, the microplane strain increments are evaluated by using eqns (1)–(4) then the microplane stresses are computed using the stress–strain laws defined at the microlevel, and finally the new macroscopic stress tensor is obtained by integration of microplane stresses according to eqn (5).

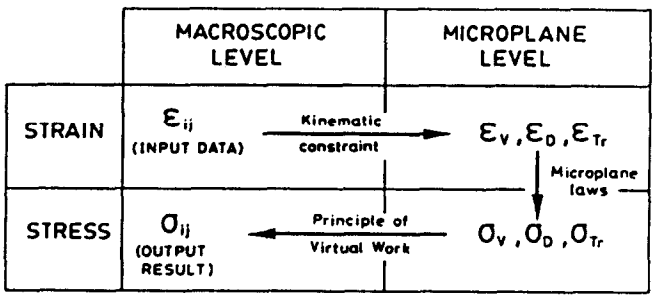


Fig. 1. Basic scheme for the computation of macroscopic stresses from the macroscopic strains.

Although not always necessary, in certain situations (e.g. as a part of a F.E. program), it is useful to calculate additionally the macroscopic tangential stiffness tensor $D_{ijkl}$, relating macroscopic stress and strain increments. In particular, this tensor is required to obtain the tangential stiffness matrix of the structure whose eigenvalues decide path bifurcations and determine the stable paths (Bažant, 1988; de Borst, 1987). The expressions for $D_{ijkl}$ can be easily derived from the incremental counterpart of eqn (5) by substituting for the microplane stresses their expressions in terms of microplane strains and then, for the microplane strains their expressions in terms of the macroscopic strains. However, since the resulting stiffness expression can be different depending on the type of stress–strain laws used at microplane level, this derivation will be given in Section 2.4, after the definition of the microplane laws.

2.2. *Constitutive relationships used at the microplane level*

Within the basic framework presented, a very wide range of models can still be defined depending on how the microplane stress–strain relationships are chosen. In this work, the laws for $\sigma_V$, $\sigma_D$ and $\sigma_T$, have been selected on the basis of those used in previous versions of the microplane model (Bažant and Prat, 1988) but with some modifications and new dependencies so as to make numerical implementation more convenient.

(a) *Volumetric law*. This microplane law directly reproduces the macroscopic behavior of the material when only volumetric strains or stresses are present. Therefore, a curve that fits experimental data for hydrostatic tests may be directly introduced. For compression ($\sigma_V > 0$) the following law is assumed:

$$\sigma_V = E_V^0 \varepsilon_V \left[ \left( 1 + \frac{|\varepsilon_V|}{a} \right)^{-p} + \left( \frac{|\varepsilon_V|}{b} \right)^{q} \right] \tag{6}$$

while for hydrostatic tension ($\sigma_V < 0$)

$$\sigma_V = E_V^0 \varepsilon_V \, e^{-(|\varepsilon_V|/a_1)^{p_1}} \tag{7}$$

where $E_V^0$, $a$, $b$, $p$, $q$, $a_1$, $p_1$ are empirical material constants obtained by fitting a single experimental curve. The volumetric law is plotted in Fig. 2a. For unloading–reloading, both the tensile and compressive curves act as envelopes. In compression the unloading branches are assumed to always have the initial slope $E_V^0$, and the origin of the tensile part of the diagram always shifts to the point in which the unloading compressive branch reaches the horizontal axis. The unloading–reloading in tension is assumed to follow a secant slope between the maximum point reached in the tensile curve and the origin of that curve.

(b) *Normal deviatoric law*. This law is based on the same type of exponential stress–strain envelope curve used for the tensile part of the volumetric behavior, but now considering two different sets of parameters for tension and compression

$$\sigma_D = E_D^0 \varepsilon_D \, e^{-(|\varepsilon_D|/a_1)^{p_1}} \quad \text{if } \sigma_D < 0 \tag{8}$$

$$\sigma_D = E_D^0 \varepsilon_D \, e^{-(|\varepsilon_D|/a_2)^{p_2}} \quad \text{if } \sigma_D \geq 0 \tag{9}$$

where $E_D^0$, $a_1$, $p_1$, $a_2$, $p_2$ are empirical material constants. The law is represented in Fig. 2b. For unloading–reloading, straight lines are assumed with a certain slope. For compressive behavior the initial slope $E_D^0$ is always used, while a secant slope (from the origin to the point of maximum positive strain previously reached) is used on the tensile side of the diagram. For unloading in compression, the origin of the tensile part of the diagram is always assumed to shift to the point in which the unloading compressive branch intersects the horizontal axis.

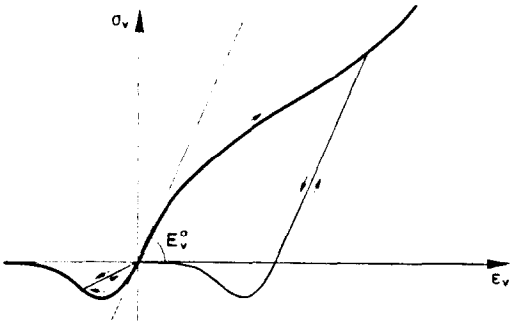


a) Volumetric stress-strain relationship

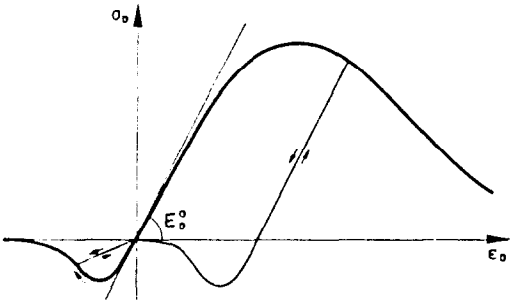


b) Normal deviatoric stress-strain relationship

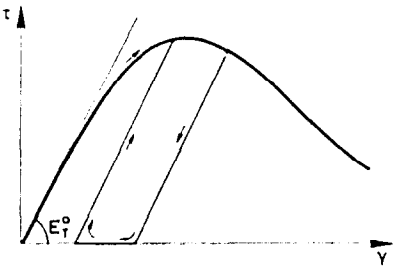


c) Tangential stress-strain moduli relationship

Fig. 2. Stress–strain laws at the microplane level.

(c) *Tangential (shear) law*. This is the most complicated among the three microplane constitutive laws. The complexity comes from two facts: first, the tangential stress and strain have two in-plane components each on the microplane and, therefore, the stress–strain law must be two-dimensional, that is, it must provide a coupled relation between two components of stress and two components of strain simultaneously. Second, in this law there must also be an additional dependence on a macroscopic variable giving a measure of the external confining pressure such that the tangential response is stiffer when the confinement is higher. This is to reflect in some way the phenomenon of internal friction, which must be taken into account if the model is expected to fit, with the same set of material parameters, the experimental data for different confinement pressures.

Several possibilities can be considered to formulate such a model in a consistent way. One of them might be to adopt a general two-dimensional plastic model similar to the ones already existing for the behavior of joints or interfaces (Gens *et al.*, 1989). However, although this kind of model would be fully consistent and satisfy all the requirements mentioned, the complexity and computational demand of such a model running at the same time on every one of the microplanes used for the numerical integration over the hemisphere would seriously reduce numerical efficiency.

Among other alternatives considered, the basic scheme proposed by Bažant and Prat (1988) seems to remain the best compromise between performance and cost, though some

important improvements concerning the influence of the macroscopic confinement may be introduced. Basically, this approach, which we call "parallel tangential hypothesis", consists of the simplifying assumption that the tangential stress vector on a microplane, $\sigma_{T_r}$, remains always parallel to the corresponding tangential strain vector, $\varepsilon_{T_r}$. This means that

$$\sigma_{T_r} = \tau \frac{\varepsilon_{T_r}}{\gamma} \tag{10}$$

where $\tau = \sqrt{\sigma_{T_r}\sigma_{T_r}}$ and $\gamma = \sqrt{\varepsilon_{T_r}\varepsilon_{T_r}}$. Then the problem reduces to establishing a one-dimensional relation between the tangential stress and strain moduli $\tau$ and $\gamma$. The relationship we use for that purpose is an exponential curve similar to that used for the other microplane laws:

$$\tau = E_T^0 \gamma e^{-(\gamma/a_3)^{p_3}} \tag{11}$$

in which $E_T^0$ and $p_3$ are empirical material constants and $a_3$ is a certain empirical function.

As shown in Fig. 2c, the curve given by this equation is used as an envelope, with unloading–reloading branches with initial stiffness $E_T^0$. Zero tangential stress is assumed when the horizontal axis is reached during unloading. For reloading, the full initial stiffness applies again up to the current envelope. In this way, a very simple loop is obtained at this level, which seems to be sufficient for obtaining a reasonable simplified approach to unloading–reloading loops at macroscopic level, as shown in one of the examples of application later in this paper.

As described so far, however, the tangential stress–strain relation would not show any dependence on the macroscopic confinement. This dependence is introduced through the parameter $a_3$ in eqn (11), which is assumed to have increasing values depending on the macroscopic confinement. In this work we take the variable $\varepsilon_V$ as the measure of the external confinement instead of $\sigma_C = (\sigma_{II}+\sigma_{III})/2$ which was used in the original formulation (Bažant and Prat, 1988). This assumption has the advantage that it makes the model fully kinematically constrained. A linear variation is assumed for the dependence of $a_3$ on $\varepsilon_V$ (Fig. 3):

$$a_3 = a_3^0 + k_a \varepsilon_V \tag{12}$$

where $a_3^0$ and $k_a$ are empirical material constants.

The fact that $a_3$ depends on $\varepsilon_V$ introduces the necessity of some additional assumptions on how to compute the stress $\tau$ from the strain $\gamma$ in Fig. 2c. In this work, the following procedure is used: first, the increment of $\tau$ is computed elastically from the increment of $\gamma$ on the basis of the initial modulus $E_T^0$. Then the curve given by eqn (11) with a value of $a_3$ corresponding to the final value of $\varepsilon_V$ is used as a limit envelope for $\tau$. As described, this procedure is based only on the total values of the variables at the end of the load step, not involving, therefore, any numerical integration procedure with sub-stepping. This feature is an apparently minor but practically important modification of the previous version of

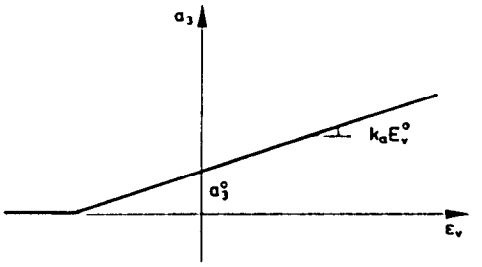


Fig. 3. Dependency of $a_3$ on $\varepsilon_V$.

the model (in which the numerical integration procedure was needed); it makes possible a fully explicit computation of a strain-prescribed load step, which is one of the objectives of this work.

### 2.3. *Path-dependence*

As is clear from eqns (6)–(12), the microplane stress–strain relations are total-strain relations which are path-independent for the case of monotonic loading on the microplane. It is important to note, however, that the macroscopic response for macroscopically monotonic loading is path-dependent. The reason is that even such loading normally involves unloading (for volumetric or deviatoric curves) or change of direction (for shear) on some microplanes. As in the previous microplane model, it is assumed that all the macroscopic path-dependence stems from the possibility of various combinations of loading and unloading on the microplanes.

This is an attractive simplifying theoretical feature of the model. In practice, however, some numerical precautions must be taken due to the numerical scheme used, explained in Section 3. According to the kinematic micro–macro constraint assumed, the change of direction of the microplane strains must come from a change in direction of the macroscopic strains. As will be shown in Section 3, the increments of strains, stresses and other variables are calculated for each load step within a loop over the number of external load steps. In the (macroscopic) strain space, the strain increment corresponding to a load step is represented by a straight segment, and the segments of the subsequent load steps constitute a polygonal approximation to the true strain path. In general, the true strain path will be a curve not necessarily smooth (e.g. consider the sudden development of lateral dilatancy in a uniaxial test near the peak, as in the first example presented in Section 4). Consequently, it is clear that in practice the load history must be divided into a sufficient number of load steps so that the true strain path and, therefore, the corresponding loading unloading combinations in the microplanes, can be captured in the calculations.

### 2.4. *Tangent macroscopic stiffness tensor*

For the derivation of the macroscopic tangent stiffness matrix, eqn (5) must be rewritten in terms of the differential stress increments instead of the total values:

$$d\sigma_{ij} = d\sigma_V \delta_{ij} + \frac{3}{2\pi}\int_\Omega d\sigma_D n_i n_j \, d\Omega + \frac{3}{2\pi}\int_\Omega \frac{d\sigma_{T_r}}{2}(n_i\delta_{rj} + n_j\delta_{ri} - 2n_i n_j n_r)\, d\Omega. \tag{13}$$

Then the increments of stresses at the microplane level must be replaced by their incremental expressions in terms of the current tangent modulus and the increments of strain at that level. These are simple scalar expressions for $d\sigma_V$ and $d\sigma_D$,

$$d\sigma_V = E_V^{tan}\, d\varepsilon_V \tag{14}$$

$$d\sigma_D = E_D^{tan}\, d\varepsilon_D \tag{15}$$

but not for $d\sigma_{T_r}$ since both the tangential stress and strain on a microplane are vectors. Their incremental relationship must involve a matrix:

$$d\sigma_{T_r} = H_{rs}^{tan}\, d\varepsilon_{T_s}. \tag{16}$$

The matrix $H_{rs}^{tan}$ for the parallel tangential model used in this work is derived in Appendix B. Its final expression involving the tangential shear stiffness $E_T^{tan}$ (obtained from the relationship $d\tau = E_T^{tan}\, d\gamma$) as well as the current values of $\sigma_{T_r}, \varepsilon_{T_r}$ and their respective moduli $\tau$ and $\gamma$, is

$$H_{rs}^{\tan} = \frac{\tau}{\gamma}\delta_{rs} + \left(E_{\mathrm{T}}^{\tan} - \frac{\tau}{\gamma}\right)\frac{\varepsilon_{\mathrm{T}r}\varepsilon_{\mathrm{T}s}}{\gamma^2}. \tag{17}$$

Introducing eqns (14)–(16) into eqn (13) and then replacing the microplane strain increments according to eqns (2)–(4), the final expression of the tangent macroscopic stiffness matrix $D_{ijkl}^{\tan}$ can be obtained. This derivation is presented in Appendix C and it requires the introduction of certain symmetry considerations for identifying the matrix coefficients from the resulting equation (or alternatively, the use of an *a priori* symmetrized version of eqn (2), as done in previous works) in order to get a stiffness expression that satisfies the interchangeability of stress tensor indices $i$ and $j$ and the strain tensor indices $k$ and $l$. The final expression is:

$$\mathrm{d}\sigma_{ij} = D_{ijkl}^{\tan}\,\mathrm{d}\varepsilon_{kl} \tag{18}$$

where

$$D_{ijkl}^{\tan} = \frac{E_{\mathrm{V}}^{\tan}}{3}\delta_{ij}\delta_{km} + \frac{3}{2\pi}\int_{\Omega} E_{\mathrm{D}}^{\tan} n_i n_j (n_k n_m - \delta_{km})\,\mathrm{d}\Omega$$
$$+ \frac{3}{2\pi}\int_{\Omega} \frac{H_{rs}^{\tan}}{4}(n_i\delta_{rj} + n_j\delta_{ri} - 2n_i n_j n_r)(n_k\delta_{sl} + n_l\delta_{sk} - 2n_k n_l n_s)\,\mathrm{d}\Omega. \tag{19}$$

Note that this is not the same expression as obtained by Bažant and Prat (1988), where the relationship between macroscopic strain and stress increments was $\mathrm{d}\sigma_{ij} = C_{ijkl}\,\mathrm{d}\varepsilon_{kl} + \mathrm{d}\sigma'_{ij}$ with the additional initial stress term; the tensor $C_{ijkl}$ did not have the meaning of tangential stiffness.

2.5. *Summary of the model parameters and their values*

Prior to establishing the final list of model parameters, it is useful to relate the three initial moduli of the microplane stress–strain laws $E_{\mathrm{V}}^0$, $E_{\mathrm{D}}^0$ and $E_{\mathrm{T}}^0$, which do not have any macroscopic physical meaning, to the standard elastic parameters. This can be easily achieved if we impose the condition that virgin concrete initially follows a linear elastic behavior. In that situation the behavior on any microplane is the same: linear elastic functions for $\sigma_{\mathrm{V}}$, $\sigma_{\mathrm{D}}$ and $\sigma_{\mathrm{T}}$ in terms of their respective strains with initial moduli $E_{\mathrm{V}}^0$, $E_{\mathrm{D}}^0$ and $E_{\mathrm{T}}^0$. These equations can be introduced into the integral in eqn (5), the microplane strains replaced according to eqns (2)–(4), and the integral over the hemisphere solved by hand, from which a final linear relationship between macroscopic stress and strain is obtained. By identifying the coefficients of that expression with the coefficients of Lamé's equation of elasticity, the following relations are obtained (Bažant and Prat, 1988):

$$E_{\mathrm{V}}^0 = \frac{E}{1-2\nu} \tag{20}$$

$$E_{\mathrm{D}}^0 = \eta_0 E_{\mathrm{V}}^0 \tag{21}$$

$$E_{\mathrm{T}}^0 = \frac{1}{3}\left[\frac{5(1-2\nu)}{1+\nu} - 2\eta_0\right]E_{\mathrm{V}}^0. \tag{22}$$

Thus, Young's modulus, $E$, Poisson's ratio, $\nu$, and the additional parameter, $\eta_0$, can be used as input parameters instead of the three initial moduli at microplane level. Then the program calculates the values of those moduli internally.

The final list includes a total of 14 parameters:

(i)—Elastic parameters: $E$, $\nu$ and $\eta_0$.
(ii)—Volumetric law: $a$, $b$, $p$, $q$, $a_1$ and $p_1$.

(iii)—Normal deviatoric law: $a_2$ and $p_2$.
(iv)—Tangential law: $a_3^0$, $k_a$ and $p_3$.

However, the six volumetric law parameters can be identified separately by simple curve fitting of the compressive and tensile hydrostatic stress–strain curves. Of these six parameters, five can be usually assumed to have the same values for most concretes: $a = 0.005, b = 0.225, p = 0.25, q = 2.25, p_1 = 0.5$. Constants $E$ and $\nu$ are known from elastic tests. Thus, only seven parameters need to be identified by fitting other than hydrostatic test data on the basis of eqn (6). Furthermore, experience shows that for most concretes, one can use $p_2 = p_3 = 1.5$. Consequently, there are only five parameters, $\eta_0$, $a_1$, $a_2$, $a_3^0$ and $k_a$, which must be determined to fit the experimental data for non-linear triaxial behavior curves. Moreover, in the case of tests with negligible confining pressure, $k_a = 0$ can be used and the number of parameters is reduced to only four. With only five or four unknown parameters, the fitting of non-linear triaxial test data is not difficult.

## 3. NUMERICAL IMPLEMENTATION

We now present a unified scheme for two computer programs serving the purposes of both "single-point" constitutive verification and F.E. structural analysis. This scheme involves two (constitutive) model-independent main programs and one (constitutive) model-specific set of subroutines.

### 3.1. *Flowcharts for constitutive verification and F.E. analysis*

Figure 4a shows the basic flowchart of the "single-point" main program developed for constitutive verification, and Fig. 4b the same scheme for the companion F.E. main program. Both diagrams present a similar structure, though the F.E. program obviously includes all the additional operations for calculating element stiffness matrices, etc. After the general data input, a first loop over the number of load steps can be observed in both programs. For the finite element program, a load step consists, as usual, of a set of applied loads and prescribed nodal displacements, while for the single-point program a load step consists of a set of values of either prescribed stress or prescribed strain for each of the six degrees of freedom considered at the constitutive level.

In both programs, the non-linear analysis of each load step is carried out by using a standard iterative initial-stress type strategy. This is reflected in the flowcharts with the inner loop controlled by an IF statement at the bottom of the diagrams. As a consequence of using the same non-linear strategy, the same type of constitutive computations are required for an iteration in both programs. Those computations are of the prescribed strain type, i.e. knowing the previous (initial) state and the values of a prescribed strain increment, the new final state (including the new values of stresses) must be obtained.

Note that the single-point main program of Fig. 4a deals directly with the components of strain and stress at a point of the material. In general, similar results can be obtained using a finite element program with a single element. However, there may be differences between the two types of analysis when stress (and not only strain) is prescribed to some of the degrees of freedom. Then, if unexpected results are to be interpreted, it becomes difficult to distinguish whether they are due to the constitutive model itself or to spurious or non-spurious but unexpected behavior of the finite elements (it is possible to obtain apparently correct but misleading results from F.E. computations with one or few elements, since the method is expected to converge to the solution of the physical problem studied only when the mesh is fine enough).

The unified implementation of the computational schemes for constitutive verification and for F.E. analysis, has important advantages which in general are clear to the specialists on large-scale computer programming, but seem to be unappreciated by many solid mechanicists who specialize in material modelling. One obvious advantage of the unified scheme presented here is that a single subroutine (or set of subroutines) for the constitutive model needs to be developed for both levels of analysis. This subroutine (or set of subroutines) can be debugged and tested with the single-point main program, and then, after this phase

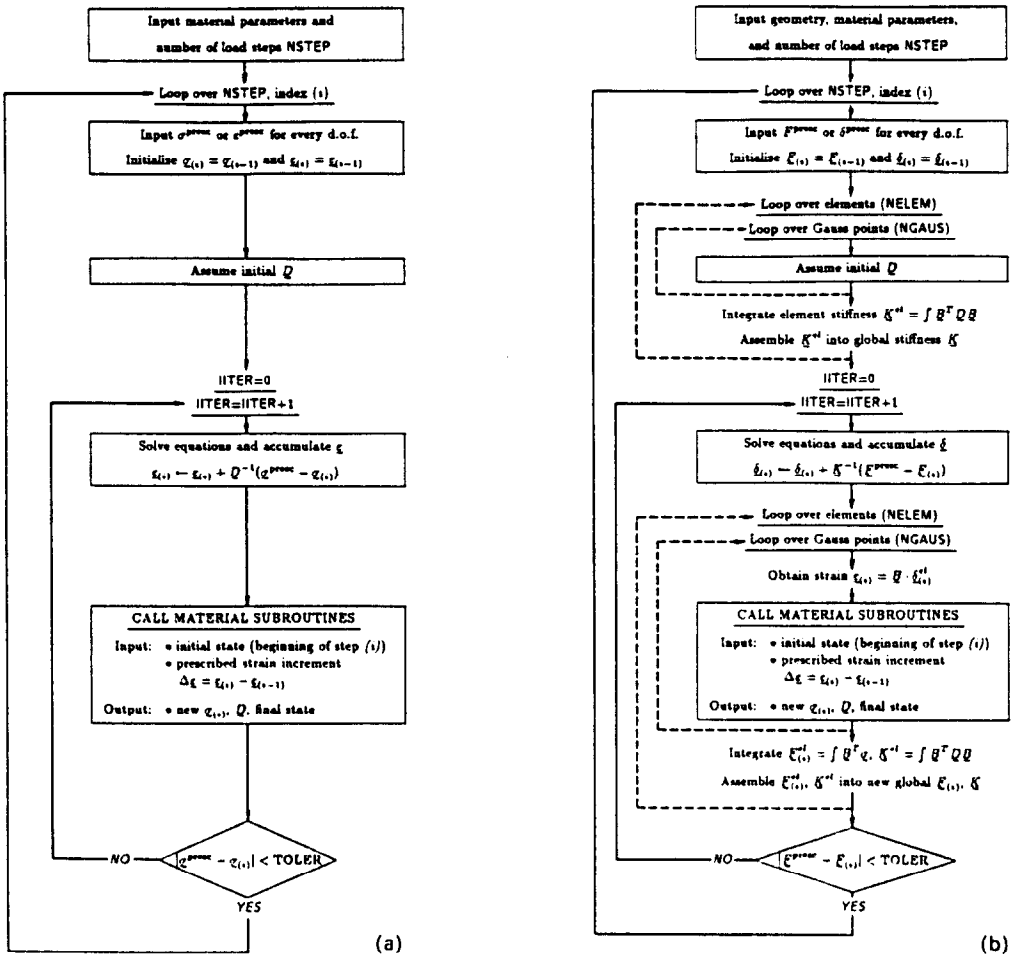


Fig. 4. (a) Basic flowchart of the 1-point constitutive verification main program. (b) Basic flowchart of the F.E. main program.

of the work has been finished, the model is automatically ready as an additional option in the general F.E. code. There are other advantages: (1) From the viewpoint of the constitutive model, the single-point main program described is general in the sense that any combination of either prescribed strain or prescribed stress for every d.o.f. is possible, and that this combination can vary from load step to load step. Therefore, any imaginable load history (with either stress or strain prescribed for every d.o.f.) can be analyzed with this program. (2) The constitutive subroutines for both (single-point and F.E.) main programs can be considered as a "black box" called only from one point in the program. Therefore, these programs are independent of the constitutive model used except for that line, which enables the same single-point main program to be used with different constitutive models. This can be easily done by replacing the CALL statement or, alternatively, making all the statements of CALL to the different models available within an IF structure. The scheme suggested also makes it easy to implement several constitutive models in the same F.E. program, as options that can be used alternatively or simultaneously in different parts of the discretization.

### 3.2. *The microplane subroutine*

In the context of the unified scheme presented above, the subroutine implementing the constitutive model itself necessitates that only the following type of computations be performed: given a certain "initial state" and a certain strain increment, the resulting final values of stress and other variables defining the new "final state" at the end of the increment

must be computed. A basic description of the steps to follow in this type of computation has already been given in Section 2.1 and Fig. 1. However, for the implementation in a practical computer subroutine, some additional numerical procedures need to be established first.

The first one is the integration over the hemisphere necessary to obtain the macroscopic stress and stiffness from the stresses and stiffnesses at the microplane level as shown in eqns (5) and (19). Following Bažant and Prat (1988), this integration is performed numerically, as a summation of the value of the function to be integrated in a number of selected "directions" $n_i$ (points on a hemisphere), each with its corresponding weight coefficient. A rule with a total of 28 integration points (or directions) distributed over the upper hemisphere (Stroud, 1971) has been adopted in this paper. However, a slightly less accurate formulation (Bažant and Oh, 1985) with 21 points could also be adequate.

The state variables in this version of the model, for both macroscopic and microplane levels include:

(i)—The macroscopic strain tensor ($\varepsilon$, a total of six variables).
(ii)—Two history variables (maximum and minimum $\varepsilon_V$ achieved so far) for the volumetric microplane stress–strain law, same for all the 28 microplanes; a total of two variables.
(iii)—Two history variables (maximum and minimum $\varepsilon_D$ achieved so far) for the normal deviatoric microplane stress–strain law, different for each one of the 28 microplanes; a total of 56 variables.
(iv)—One history variable (maximum $\varepsilon_T$) for the tangential microplane stress–strain law, different for each one of the 28 microplanes; a total of 28 variables.

This makes a grand total of 92 state variables which must be stored and updated at each load step during the computation of the stress history from the strain history at a material point (for the slightly less accurate integration formula with 21 points, this would decrease to 71 variables).

The general flowchart of the computer subroutine implementing the constitutive model for strain-to-stress calculations is represented in Fig. 5. One can see that the flowchart has a simple structure with a single loop over the number of all microplanes considered for the integration rule, 28 in the present formulation. Then the microplane strains are computed, and the corresponding laws are used to obtain the new microplane stresses, stiffnesses and history variables. This is done only once (outside the loop) for the volumetric law, since the volumetric behavior is the same for all the microplanes, and as many times as the number of microplanes (inside the loop) for the normal deviatoric and tangential laws. Finally, the integration over the hemisphere is performed and the new macroscopic stress and stiffness values for the end of the load step obtained.

The most important feature of the present scheme is that the computation of the model response under a strain-prescribed load step is fully explicit, i.e. no substepping and numerical integration is necessary within the load step for obtaining the new stress and history variables at the end of the step. Among all the new theoretical and numerical aspects of this version of the model, there are three that make it possible to achieve this: (i) the model is fully kinematically constrained, so the increments of microplane strains can be computed directly from the prescribed increment of macroscopic strain (including $\varepsilon_V$); (ii) the stress strain relationships at the microplane level are also explicit under any type of macroscopic loading, so the new values of stresses at the microplane level can be computed from the microplane strains (even $\sigma_T$, for non-constant $\varepsilon_V$); and (iii) the integral of the microplane stress over the hemisphere is expressed in terms of the total values of stresses and so the new total value of the macroscopic stress tensor can be obtained by integration of the microplane stresses.

## 4. EXAMPLES OF APPLICATION

The first example presented in this section corresponds to a uniaxial compression test carried out by van Mier (1984), in which both longitudinal and transverse strains were

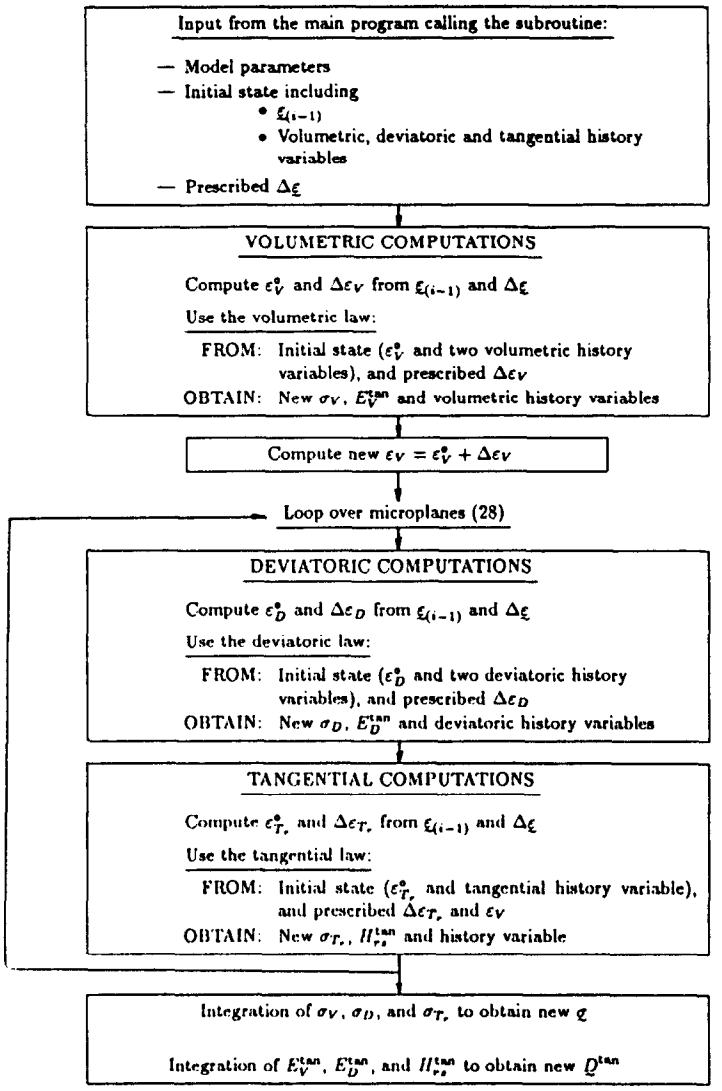


Fig. 5. Flowchart of the explicit microplane model subroutine.

measured. These measurements include the post-peak softening of the specimens—a difficult aspect whose complete description would require a very complex analysis of triaxial strain localization in the specimens. The softening may have caused the strain state in these specimens to become non-uniform after the peak load, although no observations to this effect were documented. Since evidence is lacking, the tests with post-peak softening are here analyzed under the hypothesis of uniform strain. This hypothesis is applicable only to sufficiently small specimens whose size is approximately equal to the characteristic length of the material used in non-local formulations (Bažant and Ožbolt, 1990). If the strain localized, the post-peak stress–strain curve of the material would decline less steeply than shown in Fig. 2 (and would yield a higher value of energy dissipation, which means the present analysis is on the safe side with respect to energy dissipation). The present model could then be adjusted to describe it correctly. It should further be noted, though, that even if the strain in these specimens was localized, the average stress–strain relation obtained can still be used for an approximation of finite elements of nearly the same size as the specimens tested [this is exactly true if the structural action can be approximated by the series coupling model; see Bažant and Cedolin (1991), Chapter 13]. Analysis of strain localization in the specimens tested is beyond the feasible scope of this paper.

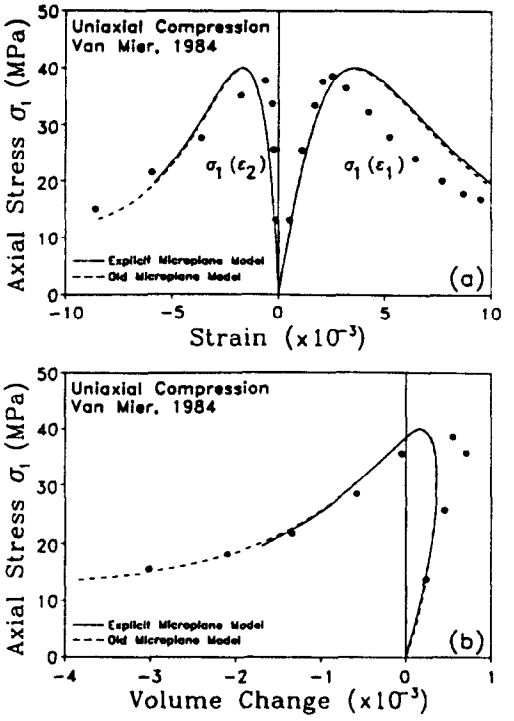


Fig. 6. Comparison with uniaxial test by van Mier (1984).

Comparisons of the present model (solid curves) with van Mier's measurements (data points) are shown in Figs 6a and 6b, the first including the axial stress–strain curve and axial stress–lateral strain curve, and the second the axial stress–volumetric strain curve. In these diagrams, the results obtained with the new explicit microplane model are represented by the solid lines, while the dashed lines are the results obtained with the previous version of the microplane model already published by Bažant and Prat (1988). The circles denote experimental data. The prescribed strain on the loading axis was applied in 15 increments of 0.0005 for the first 10 increments and 0.0010 for the remaining five. The parameter values used in this case are $E = 2406$ MPa, $\nu = 0.18$, $\eta_0 = 0.85$, $a_1 = 0.0004$, $a_2 = 0.0043$, $a_3^0 = 0.0018$, $k_a = 0$. The remaining parameters have their general values already specified.

Since $k_a = 0$, the parameter $a_3$ is assumed to be constant as it was in Bažant and Prat (1988). In this particular situation both versions of the model are equivalent from a theoretical point of view. The values of the remaining parameters in this example are also the same, which explains why the curves shown in the figure are almost coincident.

However, there is one large difference: the amount of computer time spent on calculations in both cases. In the old microplane model, a step by step numerical integration was performed within each load step, which in general is a very expensive procedure, while in the new explicit formulation, the same final values are directly obtained by means of a set of explicit expressions previously integrated by hand.

In order to make a comparison between the computer time spent with each version of the model under similar conditions, a new implementation of the old version of the microplane model has also been made. The original subroutine has been modified so that it performs the type of strain-to-stress constitutive calculations needed to be used in conjunction with the same "single-point" main program as the new explicit formulation. Then both models can be used to solve the same example under almost identical conditions and an objective evaluation of the true savings obtained with the new formulation can be made.

For any step-by-step integration procedure, the subroutine implementing the old version of the model includes a parameter that gives the measure of "how fine" the substepping within the prescribed load step will be. In that subroutine, a parameter called EPSINC is used for that purpose: any strain-prescribed load step to be computed by the subroutine is

divided in a number of proportional substeps so that the largest component of the strain tensor in one substep would not be larger than EPSINC. If EPSINC is very small, then the number of substeps is large and the integration more precise but expensive. If, on the other hand, EPSINC is given a larger value, the integration is cheaper but the error increases.

For the purpose of comparison, the same example as described in Fig. 6 was also computed several times using the old formulation with different values of EPSINC. The results obtained using the old formulation with EPSINC values of 0.0001, 0.00003 and 0.00001 are summarized in the first three columns of Table 1, together with the results obtained using the new explicit formulation in the fourth column.

The first four rows in Table 1 contain information about the CPU time spent in the computations, and the last four about the accuracy obtained in the results. The CPU times are given in terms of total values (row 1) and average CPU time spent each time the constitutive subroutine is called (row 4), since the total number of times the subroutine is called (row 3) is not the same for each run (it depends on the number of iterations necessary for each load step to converge in the single-point main program, see Fig. 4). Also, the ratio of the CPU time spent in the three calculations with the old version of the model to the time spent by the explicit formulation is given (rows 2 and 5) in the table. The comparison of accuracy is made in terms of the stress obtained at strains 0.0035 (approximately the peak strain, row 6), and 0.007 (about twice the peak strain, row 8). Assuming the values of stress computed with the explicit formulation to be the exact solution, the integration errors for the computations with the old incremental model have also been obtained (see rows 7 and 9).

From the results shown in the table it is apparent that the explicit formulation is much faster than the old incremental formulation, and the computer time is reduced dramatically. The exact value of the reduction factor depends on which of the three runs of the old model is compared, but it can very well be greater than 10 for "reasonable" integration errors under 1%, in the example studied. It must also be pointed out that under some other types of loading in which the amount of strain prescribed to the material is larger than in the example analyzed (e.g. uniaxial loading after application of a high confining pressure), the CPU time reduction could be even larger than evaluated, since the number of integration substeps increases proportionally to the step size, while the CPU time for the explicit formulation only depends on how many load steps are considered in the computation.

The second example presented in this section corresponds to a uniaxial compression test carried out by Hognestad *et al.* (1955). The results are represented in Fig. 7. The parameter values are $E = 3866$ ksi, $\nu = 0.18$, $\eta_0 = 0.5$, $a_1 = 0.00005$, $a_2 = 0.0025$, $a_1^0 = 0.0015$ and $k_u = 0$. The remaining parameters have their general values. In this example, the uniaxial strain is first increased up to 0.0028 (somewhat beyond the peak), then it is decreased to 0.001 and again increased to the final value of 0.0040, all in load steps 0.0002 in size.

The envelope curve in Fig. 7 agrees very well with the old curve and with experimental data as well, and also a reasonable shape for a basic quasi-static loop is obtained at this stage. It may be remarked that it is not a specific purpose of this work to model loops accurately. Rather, the purpose here is merely to show that reasonable (or at least not meaningless) results are obtained in the case of a load reversal.

Table 1. Comparison between the performances of the old and new formulations of the microplane model

| Step size | Old incremental model 0.0001 | 0.00003 | 0.00001 | Explicit model |
|---|---|---|---|---|
| Total CPU to $\varepsilon = 0.01$ | 61.6 s | 156.2 s | 418.9 s | 11.13 s |
| Ratio to explicit | 5.5 | 14.0 | 37.6 | 1 |
| Calls to constitutive equations | 222 | 206 | 197 | 193 |
| CPU time per call (s) | 0.277 | 0.757 | 2.130 | 0.057 |
| Ratio to explicit | 4.9 | 13.3 | 37.3 | 1 |
| $\sigma$ at $\varepsilon = 0.0035$ (MPa) | 39.00 | 39.77 | 40.05 | 40.10 |
| Error to explicit (%) | 2.74 | 0.32 | 0.12 | 0 |
| $\sigma$ at $\varepsilon = 0.007$ (MPa) | 28.24 | 29.22 | 29.58 | 29.76 |
| Error to explicit (%) | 5.11 | 1.85 | 0.60 | 0 |

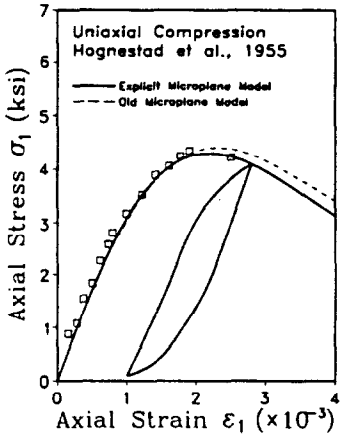


Fig. 7. Comparison with uniaxial test by Hognestad *et al.* (1955) and simple loop obtained with the new model.

In the last two examples, similar load histories consisting of two load steps are considered. During the first load step, certain confining pressure is applied to the concrete, and then a second load step consisting of a uniaxial strain increment under constant lateral pressure is applied. These examples correspond to two series of standard triaxial tests carried out by Balmer (1949) and Kotsovos and Newmann (1978). In both cases, several tests under different confining pressures are modelled; see Figs 8–9. The values of the parameters are: for Balmer, $E = 3500$ ksi, $\nu = 0.18$, $\eta_0 = 0.85$, $a_1 = 0.00005$, $a_2 = 0.001$,

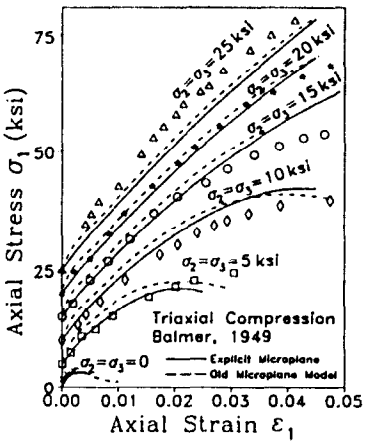


Fig. 8. Comparison with triaxial tests by Balmer (1949).

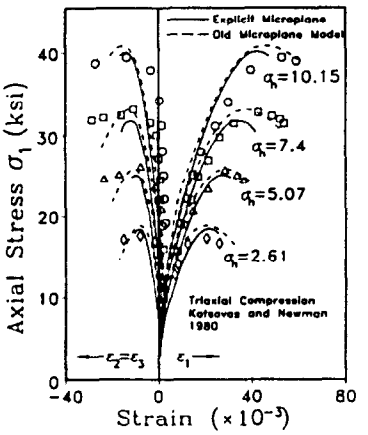


Fig. 9. Comparison with triaxial tests by Kotsovos *et al.* (1978).

$a_3^0 = 0.0025$, $k_a = 3.28$; and for Kotsovos and Newmann, $E = 3400$ ksi, $\nu = 0.18$, $\eta_0 = 0.85$, $a_1 = 0.00005$, $a_2 = 0.002$, $a_3^0 = 0.008$ and $k_a = 0.61$. All the remaining parameters have their general values.

The objective of these two examples is to demonstrate that the new explicit formulation can also reproduce satisfactorily the behavior of concrete under different confining pressures, as can be seen in the figures. This is an important achievement, since it is in this part of the model (influence of external confinement on microplane laws) in which the main theoretical change has been made compared to the old microplane model.

## 5. SUMMARY AND CONCLUSIONS

While the aim of the original development of the microplane model had been the accuracy in the modelling of test results, the main objective of the present new version of the model is to achieve a new more rational and comprehensive theoretical description of the model, as well as an easy implementation in a general code and numerical efficiency in large-scale computations. To this end, the basic hypotheses have been reviewed, some expressions have been rewritten in terms of total values rather than differential increments of the variables, and a few important changes have been made in the functions and internal dependences assumed. Also, physical interpretation has been provided for the variables and equations whenever possible. On the numerical side, the model has been implemented in a subroutine capable of performing explicit strain-to-stress calculations. This subroutine can be used in either of two main programs, one for constitutive verification and the other for F.E. analysis. The examples of application show that the new explicit formulation gives a very important reduction in computer time (one order of magnitude compared with the same case analyzed using the previous version of the model). The explicitness of stress calculation also eliminates the problem of error accumulation during the numerical integration. These practical advantages together with the good qualitative agreement of the model with a wide range of experimental results in the full three-dimensional domain make attractive the use of the model in the context of general F.E. codes and practical structural computations.

*Acknowledgements*—Partial financial support has been obtained for material modelling from AFOSR under contract No. F49620-87-C-0030DEF with Northwestern University, and for numerical implementation under U.S. NSF grant MSM-8700830. The first author is grateful for financial support under a NATO fellowship and the second author for a fellowship from the Ministry of Education of Spain. Partial support from the Spanish CICYT under research projects PA85-0321 and PB87-0861 is also gratefully acknowledged. The authors also wish to thank the Civil Engineering Department and the Center for Advanced Cement-Based Materials at Northwestern University for providing a stimulating environment for research and discussion.

## REFERENCES

Balmer, G. G. (1949). Shearing strength of concrete under high triaxial stress—computation of Mohr's envelope as a curve. Structural Research Laboratory Report No. SP-23, Denver, Colorado.

Batdorf, S. B. and Budianski, B. (1949). A mathematical theory of plasticity based on the concept of slip. National Advisory Committee for Aeronautics (N.A.C.A.), Technical Note No. 1871, Washington, DC.

Bažant, Z. P. (1984). Microplane model for strain-controlled inelastic behavior. In *Mechanics of Engineering Materials* (Edited by C. S. Desai and R. H. Gallagher), Chap. 4, pp. 45–59. John Wiley & Sons, Chichester and New York.

Bažant, Z. P. (1988). Stable states and paths of structures with plasticity or damage. *J. Engng Mech., ASCE* **114**(12), 2013–2034.

Bažant, Z. P. and Cedolin, L. (1991). *Stability of Structures: Elastic, Inelastic, Fracture and Damage Theories*. Oxford University Press, New York.

Bažant, Z. P. and Gambarova, P. G. (1984). Crack shear in concrete: crack band microplane model. *J. Struct. Engng, ASCE* **110**(9), 2015–2035.

Bažant, Z. P. and Oh, B. H. (1983). Crack band theory for fracture of concrete. *Matériaux et Constructions* **16**(93), 155–177.

Bažant, Z. P. and Oh, B. H. (1985). Microplane model for progressive fracture of concrete and rock. *J. Engng Mech., ASCE* **111**(4), 559–582.

Bažant, Z. P. and Ožbolt, J. (1990). Nonlocal microplane model for fracture, damage and size effect in structures. *J. Engng Mech., ASCE* **114**(11), 2485–2505.

Bažant, Z. P. and Prat, P. C. (1988). Microplane model for brittle-plastic material—I. Theory—II. Verification. *J. Engng Mech., ASCE* **114**(10), 1672–1688.

de Borst, R. (1987). Stability and uniqueness in numerical modelling of concrete structures. *IABSE Colloquium Computational Mechanics of Concrete Structures*, Delft, The Netherlands, 1987. IABSE Report No. 54, 161–176.
Gens, A., Carol, I. and Alonso, E. E. (1989). Elasto-Plastic model for joints and interfaces. *Proceedings, Second Int. Conf. on Computational Plasticity*, Barcelona, Spain. (Edited by D. R. J. Owen, E. Hinton and E. Oñate, pp. 1251–1264. Pineridge Press, Swansea.
Hognestad, E., Hanson, N. W. and McHenry, D. (1955). Concrete stress distribution in ultimate strength design. *J. Am. Concr. Inst.* **52**(4), 455–477.
Kotsovos, M. D. and Newmann, J. B. (1978). Generalized stress–strain relations for concrete. *J. Engng Mech., ASCE* **104**(4), 845–856.
van Mier, J. G. M. (1984). Strain-softening of concrete under multiaxial loading conditions. Ph.D. Dissertation, Univeristy of Eindhoven, The Netherlands.
Pande, G. N. and Sharma, K. G. (1983). Multilaminate model of clays—a numerical evaluation of the influence of rotation of principal axes. *Int. J. Numer. Anal. Methods Geomech.* **7**, 397–418.
Stroud, A. H. (1971). *Approximate Calculation of Multiple Integrals*. Prentice-Hall, Englewood Cliffs, NJ.
Taylor, G. I. (1938). Plastic strain in metals. *J. Inst. Metals* **62**, 307–324.
Zienkiewicz, O. C. and Pande, G. N. (1977). Time-dependent multi-laminate model of rocks—a numerical study of deformation and failure of rock masses. *Int. J. Numer. Anal. Methods Geomech.* **1**, 219–247.

## APPENDIX A: APPLICATION OF THE PRINCIPLE OF VIRTUAL WORK

Enforcing the equality of virtual work between the macroscopic stress tensor $\sigma_{ij}$ and the corresponding microplane stresses $\sigma_V$, $\sigma_D$ and $\sigma_{T_r}$, when a field of arbitrary virtual strain variations $\delta\varepsilon_{ij}$ are prescribed to the model, one obtains the equation (Bažant, 1984):

$$\frac{4\pi}{3}\sigma_{ij}\delta\varepsilon_{ij} = 2\int_\Omega [(\sigma_V + \sigma_D)\delta\varepsilon_N + \sigma_{T_r}\delta\varepsilon_{T_r}]\,d\Omega \tag{A1}$$

where the sign $\delta$ denotes the virtual variations. Given the kinematic constraint between the macroscopic and microplane strains, eqns (1) and (2) can be used for the virtual strain variations:

$$\delta\varepsilon_N = n_i n_j \delta\varepsilon_{ij} \tag{A2}$$

$$\delta\varepsilon_{T_r} = (\delta_{rk} - n_r n_k) n_l \delta\varepsilon_{kl}. \tag{A3}$$

Introducing these equations in eqn (A1), the following variational equation is obtained:

$$\sigma_{ij}\delta\varepsilon_{ij} = Y_{ij}\delta\varepsilon_{ij} \tag{A4}$$

where

$$Y_{ij} = \sigma_V\delta_{ij} + \frac{3}{2\pi}\int_\Omega \sigma_D n_i n_j\,d\Omega + \frac{3}{2\pi}\int_\Omega \sigma_{T_r}(\delta_{ri}n_j - n_i n_r n_j)\,d\Omega. \tag{A5}$$

Equation (A4) is a variational equation which must hold for any variation $\delta\varepsilon_{ij}$ but with the restriction given by symmetry ($\delta\varepsilon_{ij}$ cannot be different to $\delta\varepsilon_{ji}$). This restriction makes the direct elimination of the term $\delta\varepsilon_{ij}$ from both sides of the equation (which would lead to $\sigma_{ij} = Y_{ij}$) incorrect, since it would be equivalent to accept that symmetric terms can have independent variations. Instead, the implicit summation over $i$ and $j$ on both sides of the equation must be developed, and each pair of the symmetric terms of $\delta\varepsilon_{ij}$ and $\sigma_{ij}$ considered as a single term and their coefficients grouped. Finally the following expression is obtained:

$$\sigma_{ij} = \tfrac{1}{2}(Y_{ij} + Y_{ji}) \tag{A6}$$

from which, after substitution of $Y_{ij}$ from eqn (A5), the final eqn (5) for $\sigma_{ij}$ is obtained.

Alternatively, with intuition (Bažant and Prat, 1988), one may symmetrize in advance the tensorial expression multiplying $\delta\varepsilon_{kl}$ in eqn (A3) because the product of its nonsymmetric part with $\delta\varepsilon_{kl}$ vanishes. In that case, $Y_{ij}$ is symmetric, eqn (A4) implies that $\sigma_{ij} = Y_{ij}$ and eqn (5) results again.

## APPENDIX B: INCREMENTAL RELATIONSHIP FOR THE PARALLEL MODEL

The basic equation of the parallel model, eqn (10), can be written as:

$$\sigma_{T_r} = \frac{\tau}{\gamma}\varepsilon_{T_r}. \tag{B1}$$

By differentiation,

$$d\sigma_{T_r} = \frac{\tau}{\gamma} d\varepsilon_{T_r} + \varepsilon_{T_r} d\left(\frac{\tau}{\gamma}\right). \tag{B2}$$

The differentiation of $\tau/\gamma$ leads to

$$d\left(\frac{\tau}{\gamma}\right) = \frac{d\tau}{\gamma} - \frac{\tau\, d\gamma}{\gamma^2} \tag{B3}$$

where the increment of the shear stress modulus can be written as a product between the tangent stiffness in the $\tau-\gamma$ space (modulus to modulus relationship) and increment of shear strain modulus:

$$d\tau = E_T^{tan}\, d\gamma. \tag{B4}$$

The increment of the shear strain modulus $d\gamma$ must be related to the increment of its components $d\varepsilon_{T_r}$ as

$$d\gamma = \frac{\partial\gamma}{\partial\varepsilon_{T_r}} d\varepsilon_{T_r} \tag{B5}$$

and, since $\gamma = \sqrt{\varepsilon_{T_r}\varepsilon_{T_r}}$, the partial derivative becomes

$$\frac{\partial\gamma}{\partial\varepsilon_{T_r}} = \frac{\varepsilon_{T_r}}{\gamma} \tag{B6}$$

from which, making all the corresponding back-substitutions, the final eqn (17) is obtained.

## APPENDIX C: DERIVATION OF THE MACROSCOPIC TANGENT STIFFNESS

Introducing eqns (14)–(16) into eqn (13) and then replacing the increments of microplane strains according to eqns (1)–(4) in terms of the macroscopic strain increment $d\varepsilon_{kl}$, the following equation is reached:

$$d\sigma_{ij} = Z_{ijkl}\, d\varepsilon_{kl} \tag{C1}$$

where

$$Z_{ijkl} = \frac{E_V^{tan}}{3}\delta_{ij}\delta_{kl} + \int_\Omega E_D^{tan} n_i n_j (n_k n_l - \delta_{kl})\, d\Omega + \int_\Omega \frac{H_{rs}^{tan}}{2}(n_i\delta_{rj} + n_j\delta_{ri} - 2n_i n_j n_r)(n_l\delta_{sk} - n_k n_l n_s)\, d\Omega. \tag{C2}$$

The coefficients $Z_{ijkl}$ have been derived correctly and, if used to compute the increment of stress, they would give the correct values. However, they cannot be identified directly with the components of the tangent stiffness tensor since they do not satisfy the condition of interchangeability of indices $k$, $l$ associated with the symmetry of the strain tensor (although they do satisfy the condition for indices $i$, $j$ associated with the symmetry of the stresses). One way to identify the components of a symmetry-consistent stiffness matrix $D_{ijkl}^{tan}$, may be to replace the stress increment in eqn (C1) by its expression involving $D_{ijkl}^{tan}$, i.e.

$$D_{ijkl}^{tan}\, d\varepsilon_{kl} = Z_{ijkl}\, d\varepsilon_{kl}. \tag{C3}$$

Then the procedure to follow is to develop the summation for $k$ and $l$ on both sides, consider the symmetric components $kl$ and $lk$ of the strain tensor as a single variable, group their coefficients, and then also consider $D_{ijkl}^{tan}$ and $D_{ijlk}^{tan}$ as the same variable. The result is

$$D_{ijkl}^{tan} = \tfrac{1}{2}(Z_{ijkl} + Z_{ijlk}) \tag{C4}$$

which leads directly to the final expression of $D_{ijkl}^{tan}$ in eqn (19).